
Proceedings Paper:
Olanrewaju, F, Wu, Y, Li, H et al. (2020) An Improved Heat Release Rate (HRR) Model for the Analysis of Combustion Behaviour of Diesel, GTL, and HVO Diesel. In: SAE Technical Paper Series. SAE Powertrains, Fuels & Lubricants Meeting, 22-23 Sep 2020, Online. SAE International. Article no: 2020-01-2060. ISSN: 0148-7191. EISSN: 2688-3627.

https://doi.org/10.4271/2020-01-2060

2020-01-2060

An Improved Heat Release Rate (HRR) Model for the Analysis of Combustion Behaviour of Diesel, GTL, and HVO Diesel

Author, co-author (Do NOT enter this information. It will be pulled from participant tab in MyTechZone)

Affiliation (Do NOT enter this information. It will be pulled from participant tab in MyTechZone)

Abstract

Heat Release Rate (HRR) analysis is indispensable in engine research. The HRR of Internal Combustion Engines (ICEs) is most sensitive to gamma (γ). The proposed HRR models in literature were largely based on γ expressed as functions of temperature. However, γ is depended on temperature as well as the excess air ratio (λ). In this work, an improved HRR model based on $\gamma(T,\lambda)$ was used to investigate the combustion behaviour of standard diesel, Gas–to-Liquid (GTL) diesel and Hydrotreated Vegetable Oil (HVO) diesel in a 96 kW, multiple fuel injection, Euro V, Direct Injection (DI) engine. The improved HRR model (Leeds HRR model) was validated for the alternative fuels by comparing the fuel masses predicted by the model to the measured fuel masses. The fuel masses predicted by the Leeds HRR model were also compared to the predictions from four HRR models that were based on $\gamma(T)$. No work has been done in the past to investigate the combustion behaviour of GTL and HVO diesel in a multiple fuel injection, Compression Ignition (CI) engine. This work also featured two novel approximation techniques that were used to estimate the rate of evaporation of the injected fuel from the HRR profiles and the actual SoC from the HRR and fuel burn profiles (for the case of significant heat release bTDC). The overall average error in the predictions of the Leeds HRR model was 4.86% with a standard deviation of 2.39 while the typical error in the other models ranged from 14.66% to 19.99%. The accuracy of the HRR model of CI engines for the HRR analysis of GTL and HVO diesel is therefore, improved by using $\gamma(T,\lambda)$. The combustion of HVO diesel was found to be the smoothest of the three fuels due to the narrow distillation range of HVO diesel.

Introduction

Heat Release Rate (HRR) analysis is carried out in engine research to investigate the combustion behaviour of fuels and to enhance the thermal efficiency of Internal Combustion Engines (ICEs). Accuracy is of the essence in the development of HRR models for ICEs because the HRR of an ICE cannot be measured real–time, it can only be modelled mathematically. The ratio of specific heats, gamma (γ) is the most important thermodynamic property in the modelling of the HRR of an ICE [1] because it has the greatest impact on the accuracy of the model. The existing models of γ were largely expressed in terms of the temperature of the gases in the cylinder even though γ is known to be strongly depended on the excess air ratio (λ) of the engine. The authors of the current work have developed an HRR model, Leeds HRR, [2] that has a better accuracy in terms of the prediction of the fuel consumption compared to the experimental results (measurement). The aim of this work was to apply and validate the model to alternative fuels: Gas–to–Liquid (GTL) diesel, and Hydrotreated Vegetable Oil (HVO) diesel. HVO diesel is derived from waste cooking oil or animal fats while GTL diesel is produced from the Fischer-Tropsch process by the conversion of methane-rich gases into longer-chain hydrocarbons (liquid synthetic fuels). GTL and HVO diesels have lower engine out emissions than ULSD [3,4]. Furthermore, the two alternative fuels can be used in CI engines without modifying the existing infrastructure. GTL and HVO diesels have different distillation characteristics, though the two fuels are similar in some thermo-physical properties. The selection of the two alternative fuels for the HRR analysis in this work was based on the reasons stated above.

Previous HRR models of ICEs

The basic differences between the HRR models in literature are the γ functions and the heat transfer coefficient models that were used by the authors. Various γ models have been proposed in literature [5,6,7,8]. Gatowski, J.A., et al., [5] used a linear function of the mean charge temperature to model the specific heats ratio. The γ model of the authors was solely a function of temperature (Eq. (1)).

$$\gamma = \gamma_0 - K_1(T - T_{ref})/1000 \quad (1)$$

The reference value in Eq. (1), γ_0 = 1.38, the constant K_1 = 0.08 and the reference temperature, T_{ref} = 300 K.

Brunt, M.F.J., and Andrew, L.E., [6] evaluated the HRR of a Spark Ignition (SI) engine by using a second-order function that was derived from a multidimensional model (Eq. (2)). The γ function in their equation was evaluated as the mean function of γ functions within a narrow range of λ (0.83< λ<1.25). The γ model was based on the temperature of the gases in the cylinder, T in Kelvin.

$$\gamma = 1.338 - 6.0 \times 10^{-5}T + 1.0 \times 10^{-8}T^2 \quad (2)$$

Egnell, R., [7] proposed an exponential γ function given in Eq. (3). The exponential model in Eq. (3) is explicitly a function of temperature though the authors chose the values of the constants in the equation based on the combined effects of temperature and gas composition.

$$\gamma = \gamma_0 - k_1 \exp(-k_2/T) \quad (3)$$

The reference value in Eq. (3), γ_0 = 1.38, while the constants k_1 and k_2 have values 0.2 and 900 respectively.

Blair, G.P., [8] proposed a γ model which is specifically for exhaust gas at stoichiometric condition, equivalence ratio, $\phi = 1$ ($\lambda = 1/\phi = 1$). The model of the author is also solely depended on temperature as shown in Eq. (4).

$$\gamma = 1.4221 - 1.8752e-4T + 6.9668e-8T^2 - \cdots$$

$$-9.099 - 12T^3 \quad (4)$$

Ceviz, M.A., and Kaymaz, I. [1] derived γ functions for unburned and burned mixtures in terms of the in-cylinder temperature and λ (Eq. (5) and Eq. (6) respectively). The ranges of temperature for the unburned and burned mixtures respectively were 300 K to 1,500 K and 300 K to 2,500 K.

$$\gamma_u = a_1 + a_2T + a_3T^2 + a_4T^3 + a_5T^4 + a_6T^5 + a_7/\lambda \quad (5)$$

$$\gamma_b = b_1 + b_2T + b_3/\lambda + b_4T^2 + b_5/\lambda^2 + b_6T/\lambda + b_7T^3 + \cdots + b_8/\lambda^3 + + b_9T/\lambda^2 + b_{10}T^2/\lambda \quad (6)$$

The final derived equation of γ was expressed as given in Eq. (7).

$$\gamma = MFB\gamma_b + (1 - MFB)\gamma_u \quad (7)$$

MFB in Eq. (7) represents the Mass Fraction Burned.

The coefficients in Eq. (5) and Eq. (6) were given by the authors as shown in Table A.1.

Ceviz, M.A., and Kaymaz, I. [1] used a FIAT, 1.801 dm^3 (0.0018 m^3), four stroke SI engine to investigate the accuracy of their γ model. The engine was operated at ¾ throttle valve opening position and 2,500 rpm at λ values of 0.996, 1.089, 1.216 and 1.341. According to the authors, the proposed γ model was accurate for SI engines when λ was approximately 1.1.

The derived γ model of Ceviz, M.A., and Kaymaz, I. [1] cannot be used as it is for the analysis of the HRR of a CI engine. The authors validated the model using an SI engine operating at near-stoichiometric conditions and a single speed value (2,500 rpm). Modern diesel engines operate by the auto-ignition of compressed, lean fuel-air mixtures. Consequently, the unburned mass fraction in diesels is negligible. Burned mixtures refer to the working fluid or products of combustion in the combustion chamber during the expansion process (after the SoC) when temperatures are high (>1,700 K). Unburned mixtures refer to the working fluid during the compression stroke prior to combustion and at T<1,700 K. In both cases the fuel is assumed to be in the vapour phase [9]. Unburned mixtures are mostly applicable to SI and HCCI (Homogeneous Charge Compression Ignition) diesel engines for which fuel injection occurs during the intake stroke. The current work was carried out on a multiple fuel injection strategy CI engine (a lean combustion engine); the injected fuel mass per power stroke was injected in phases during the power stroke. The injection of fuel occurred near the TDC. The auto-ignition and combustion of the injected fuel also commenced near the TDC. The duration that the fuel-air mixture was unburned in the engine prior to the Start of Ignition (SoI) was relatively short compared to SI engines or HCCI-mode diesel engines. Therefore, burned mixture properties were assumed for the power stroke of the engine in this work. Furthermore, CI (diesel) engines operate within a much wider range of λ. For these reasons, the derived equation of Ceviz, M.A., and Kaymaz, I. [1] was modified in this work by equating MFB to 1 so that $\gamma_{mod}(T, \lambda) = \gamma_b$ (Eq. (6)).

In this work, the modified γ function, $\gamma_{mod}(T, \lambda)$ and the Leeds HRR model developed by Olanrewaju, F.O., et al., [2] were used to investigate the combustion behaviour of standard diesel (ULSD), GTL diesel, and (HVO) diesel. At low and medium loads, the effect of EGR rate on the HRR of a CI engine was found to be insignificant [2]. Therefore, EGR rate was not considered in this work. The accuracies of γ_{mod} and the γ models given in Eq. (1) to Eq. (4) to model the combustion behaviour of the three fuels were investigated by using the Leeds HRR model. The Cumulative Heat Release (CHR) profiles of the fuels were determined from the HRR curves for the engine modes that were tested. The Leeds HRR model in this work was validated for standard diesel and the alternative fuels by comparing the predicted fuel consumption to the measured fuel consumption. The validated HRR model and CHR profiles were, thereafter, used to determine the MFB profiles for the fuels and the engine modes considered in this work. The combustion behaviour of the diesel fuels and the combustion phasing parameters were determined and compared using the HRR, CHR and MFB profiles.

Methodology

Leeds CI engine HRR model development

The Leeds CI engine HRR model of Olanrewaju, F.O., et al., [2] (Eq. (8)) was used in this investigation.

$$\frac{dQ}{d\theta} = \frac{\gamma}{\gamma-1}p\frac{dV}{d\theta} + \frac{1}{\gamma-1}V\frac{dp}{d\theta} + \frac{dQ_W}{d\theta} + h_{bb}\frac{dm_{bb}}{d\theta} + q_e\frac{dm_f}{d\theta} \quad (8)$$

$\frac{dQ}{d\theta}$ = rate of release of heat energy from injected fuel, J/CAD

p = instantaneous pressure of the cylinder, Pa

V = instantaneous volume of the cylinder, m^3

$\frac{dQ_W}{d\theta}$ = heat losses through the walls, J/CAD

$\frac{dm_{bb}}{d\theta}$ = blow-by mass flow, kg/CAD

h_{bb} = enthalpy of blow-by gases, J/kg

$\frac{dm_f}{d\theta}$ = rate of evaporation of injected fuel, kg/CAD

q_e = heat of evaporation of fuel, J/kg

θ = crank angle degree (CAD)

The heat flow to the walls was calculated from Eq. (9).

$$Q_w = hA_s(T - T_{ref}) \quad (9)$$

Q_w = wall losses, J/s

h = heat transfer coefficient, W/m^2 K

A_s = total surface area of heat loss (cylinder liner area, piston surface and cylinder head above piston)

The cylinder temperature on the other hand, was estimated from the ideal gas law (Eq. (10))

$$T = pV/mR \quad (10)$$

m = amount of gas in the cylinder, kmol

R = universal gas constant, kJ/kmol K

The observed steady state temperature of the coolant/lubricant oil was used as the reference temperature in Eq. (9). The lubricant oil absorbed the heat that was transferred across the walls of the cylinder of the engine. The temperature of the lubricant was among the data that was logged during the experiment.

The blow-by rate, dm_{bb}/dt in Eq. (8) was estimated as a function of pressure from Eq. (11) and Eq. (12) [10]:

$$\frac{dm_{bb}}{dt} = A_{eff} p \left(\sqrt{2/(RT)}\right) (2/(\gamma+1))^{1/\gamma-1} \sqrt{\gamma/(\gamma+1)} \quad (11)$$

$$A_{eff} = D\pi\delta \quad (12)$$

$\frac{dm_{bb}}{dt}$ = mass flow rate, kg/s

A_{eff} = effective flow area, m^2

p = cylinder pressure, Pa

T = cylinder temperature, K

γ = ratio of specific heats

D = cylinder bore, m

δ = blow-by gap (clearance between the piston rings and the cylinder liner/wall), m. The value of δ was specified as 0.00001 m [10].

The differential, dm_{bb}/dt was converted to $dm_{bb}/d\theta$ by multiplying the equation by the appropriate conversion factor (which was a function of the speed of the engine) for each of the tested modes.

The fuel evaporation rate in Eq. (8) was estimated by using a novel approximation approach. Multiple fuel injection strategy involves three distinct injection events: pilot injection (for the control of noise and emissions), main injection and post injection. Post injection is further divided into close-post injection (for emissions control) and late-post injection (for the regeneration of aftertreatment devices) [11]. Pilot and post injection fuel masses are much less than the mass of fuel that is injected during the main injection event. The approach that was used to estimate the fuel evaporation rate in this work was based on the knowledge that each of the prominent peaks in the HRR profile of the multiple fuel injection strategy CI engine resulted from the auto-ignition and combustion of the fuel mass that was injected immediately before the peak in the preceding main injection event. Prior to auto-ignition, the injected fuel mass absorbed heat from the hot gases in the cylinder to evaporate. The HRR profile was initially modelled from the basic input data (the pressure trace) without the evaporation term of Eq. (8). The crank angle timing for each of the main injection events was meticulously determined from the HRR profiles between the estimated SoC and EoC. The heat that was released between the injection events was then determined cumulatively. The corresponding injected fuel masses were determined by dividing the estimated heat release per injection event by the calorific value of the fuel. Thereafter, the heat that was absorbed by the injected fuel from the gases in the combustion chamber to evaporate was determined by multiplying the estimated fuel masses by the heat of vaporization of the fuel. The estimated heat of vaporization for each of the injection events was incorporated into the model in Excel specifically at the crank angle of the prominent peak that was sequel to the injection (fuel injection did not occur at all the crank angles of the power stroke).

Heat transfer coefficient correlation

The heat transfer correlation of Hohenberg, G.F., [12] (Eq. (13)) was utilized in this work to calculate the HRR of the engine.

$$h = 130V^{-0.06}p^{0.8}T^{-0.4}(c_m + 1.4)^{0.8} \quad (13)$$

V, p and T are cylinder volume (m^3), pressure (Pa) and temperature (K) respectively while c_m is the mean piston speed (m/s).

Model assumptions

The following assumptions were made to develop the Leeds HRR model for the HRR analysis in this work:

1. Single zone combustion (combustion parameters were uniform in the cylinder).
2. A zero-dimensional (transient) HRR model.
3. Ideal gas behavior.
4. The injected fuel mass per power stroke was equal for all the four cylinders.
5. Evaporation of the injected fuel mass was followed by combustion [10].
6. Complete combustion of the evaporated fuel mass per injection
7. The unburned fuel mass was negligible owing to lean combustion and auto-ignition of compressed charge in diesels [2].

Engine and instrumentation

The details of the engine, instrumentation and test conditions that were used were as summarized in Tables 1, 2 and 3 below. Each of the three fuels (ULSD, GTL, and HVO diesels) was tested at the three engine test modes given in the second column of Table 3. The three engine test modes depicted in Table 3 (1,000 rpm; 30% throttle, 1,600 rpm; 50% throttle, and 1,900 rpm; 70% throttle) were chosen to represent low, medium and high power conditions in the testing matrix.

The basic model input data (the cylinder pressure-crank angle data) were measured by a pressure transducer and AVL FlexIFEM Indi 601 (2-channel). The pressure transducer was installed on the head of the first cylinder of the engine. The measured cylinder pressures were averaged over 50 cycles and logged by AVL Indicom software. The measured pressures were used in the HRR analysis that was carried out without further post-processing by filtration or averaging techniques. The HRR model was solved and analyzed in Microsoft Office Excel software.

Table 1. Engine description

Feature	Specification
Type	4-stroke, 4-cylinder CI engine
Make	IVECO, EURO V FIAT
Rated power	96 kW
Bore/Stroke	95.8 mm/104 mm (0.0958 m/0.104 m)
Compression ratio	18:1
Injection strategy	Multiple
Displacement per cylinder	749 cc (0.00075 m^3)
Total volume per cylinder	794 cc (0.0008 m^3)
Dynamometer	100 kW AC Dynamometer
Injection pressure	160 MPa (1,600 bar)

Table 2. Instrumentation

Parameter	Equipment specification
Cylinder pressure	AVL FlexIFEM Indi 601 (2-channel)
Fuel flow	Fuel meter (BC 3034)
Engine temperature	Thermocouples

Table 3. Test conditions

Test	Engine test mode	Fuel	Power, kW
1	1,000 rpm; 30% throttle	ULSD	13
2		GTL	13
3		HVO	13
4	1,600 rpm; 50% throttle	ULSD	27
5		GTL	27
6		HVO	27
7	1,900 rpm; 70% throttle	ULSD	47
8		GTL	47
9		HVO	47

Properties of fuels

The properties of the three fuels that were investigated in this work were as given in Table 4 below [11,12,13,14].

Table 4. Properties of the investigated fuels

Property	ULSD	GTL	HVO
Kinematic viscosity @ 40 °C, mm^2/s	~2.7	~3.5	2.8
Density @ 40 °C, kg/m^3	~830	762	762
Cetane number	>51	79	78.8
NCV, MJ/kg	44	44	44
Sulphur, mg/kg	<10	0.05	<1
Aromatics, wt%	11 (upper limit)	0.3	0.3

Distillation characteristics of tested fuels

The distillation characteristics of the tested fuels (ULSD, GTL, and HVO) were determined by TGA on a METTLER TOLEDO Thermogravimetric analyzer. The temperature setting that was used on the analyzer was 30 ^{0}C to 600 ^{0}C.

Determination of SoC and EoC

The CHR profiles for the tested modes were determined from the modelled HRR profiles. The fuel burn profiles were then determined from the HRR and the CHR profiles in order to determine the SoC and EoC of the tested engine modes. The SoC is defined as the point where the HRR is minimum and then followed by a sudden rise in value [15]. The crank angle at which the MFB on the fuel burn curve rose consistently above zero symbolized the actual (effective) SoC on the fuel burn profile. The EoC, on the other hand, was the crank angle at which the fuel burn profile began to level off after the MFB50.

Results and discussions

Distillation characteristics of fuels

The distillation characteristics of the tested fuels were presented graphically as shown in Figure 1.

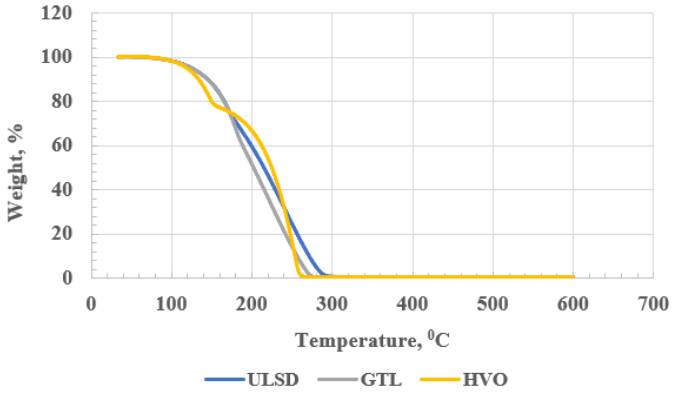

Figure 1. Distillation characteristics of ULSD, GTL, and HVO

Figure 1 showed that, although the properties of GTL and HVO diesels shown in Table 4 were similar, the alternative fuels had distinctly different distillation characteristics. As mentioned earlier, HVO diesel and GTL diesel are produced from different starting materials and by different processes. Therefore, due to the difference in the starting raw materials and the processes involved in the production of the alternative fuels, their constituent hydrocarbon fractions are not identical. Consequently, GTL and HVO diesels have different boiling ranges (distillation characteristics) as shown in Figure 1. The difference in the distillation characteristics of the two alternative fuels inadvertently implied that the two fuels would have different combustion behaviours notwithstanding the similarities in the fuel properties depicted in Table 4. Figure 1 showed that GTL diesel had the narrowest boiling range of the three fuels.

Pressure-crank angle data used as model input data

The basic input data that were used to carry out this work were the pressure traces of the engine at the specified test modes (Table 3) for each of the three diesel fuels. The input data were plotted and presented as shown in Figures 2 to 4 respectively for standard diesel, GTL diesel, and HVO diesel.

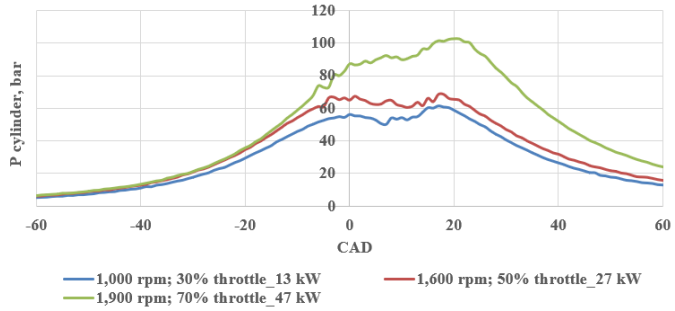

Figure 2. Pressure traces (ULSD)

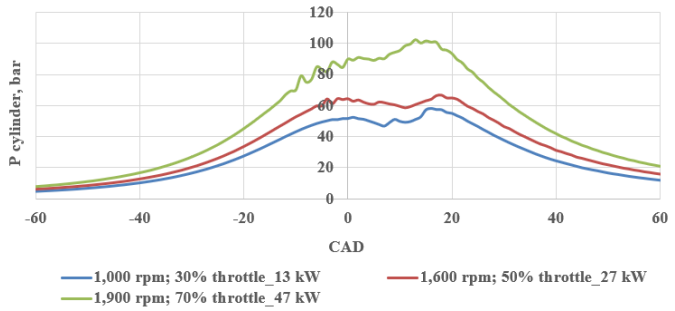

Figure 3. Pressure traces (GTL diesel)

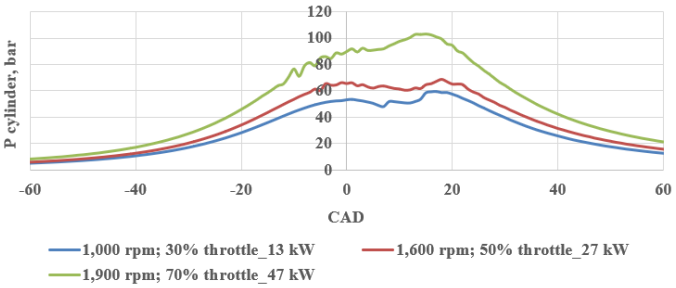

Figure 4. Pressure traces (HVO diesel)

Calculated in-cylinder temperatures

The instantaneous cylinder temperatures that were calculated from the measured in-cylinder pressures and utilized in the HRR analysis were presented graphically as shown in Figures 5 to 7 for the test conditions that were considered.

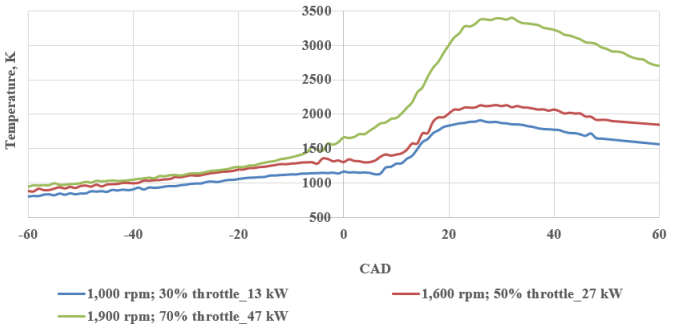

Figure 5. Calculated in-cylinder temperatures as a function of crank angle with different loads (ULSD)

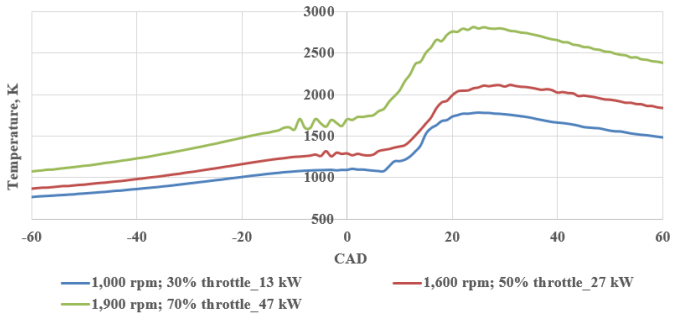

Figure 6. Calculated in-cylinder temperatures as a function of crank angle with different loads (GTL diesel)

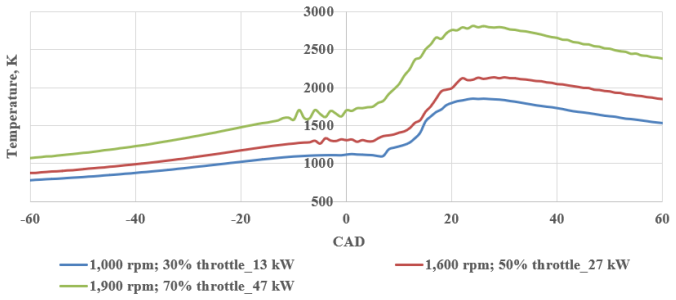

Figure 7. Calculated in-cylinder temperatures as a function of crank angle with different loads (HVO diesel)

The temperature profiles indicated that, for each of the fuels, the instantaneous in-cylinder temperature increased as the power of the engine was increased. The peak temperatures for the low, medium, and high loads occurred at crank angle degrees (CAD) of 26, 29, 32 respectively for standard diesel as shown in Figure 5. However, for the alternative fuels (GTL and HVO diesels), the peak temperatures occurred at 25, 31, 24 CAD, and 24, 28, and 25 CAD respectively for the low, medium and high power conditions (Figures 6 and 7). Therefore, the peak temperature occurred earlier when the engine was run on the alternative fuels than when it was run on fossil diesel. The early occurrence of the peak temperatures that was observed for the alternative fuels was because of the advanced Start of Injection (SoI) and the relatively high Cetane Numbers (CN) of the alternative fuels (Table 4). The SoI timings can be located on the pressure traces or temperature profiles where fluctuations were observed near the TDC. At the high power condition, much higher compression pressure and temperature were attained as shown in Figures 2 to 7. Therefore, advanced injection of fuel was triggered by the ECU of the engine at the high power conditions to prevent undesirable high PPRR and PHRR, both of which could occur should the SoI and SoC be too close to the TDC. The combined effects of advanced SoI and relatively high CN caused the auto–ignition of the compressed fuel–air mixture to occur earlier when the engine was run on GTL and HVO diesel than when it was run on standard diesel.

The pressure traces for the 3 fuels were quite similar. However, the calculated peak temperatures for the alternative fuels were lower than those of ULSD. The peak temperatures for ULSD were higher than those of the GTL and HVO diesels because of the relatively low CN and the late Start of Injection (SoI) of ULSD which meant that most of the fuel energy was released after the TDC in the case of ULSD. Due to the relatively high CN of GTL and HVO diesels as well as the advanced pilot fuel injection of the alternative fuels by the ECU, significant heat was released bTDC during the pilot combustion of the alternative fuels. This led to the observed decrease in the peak temperatures for the alternative fuels below ULSD.

The temperature profiles fluctuated near the Top Dead Centre (TDC) in Figures 5 to 7 above. The observed fluctuations were due to the auto–ignition of the pre-injected fuel while pilot injection continued. The CI engine that was used to carry out the tests was a multiple fuel injection strategy engine. Fuel injection began before the TDC in the engine and continued at specific crank angles after the TDC.

Comparison of the modified γ function and γ functions from literature for alternative fuels

The values of γ estimated from various γ functions were plotted, as depicted in Figure 8, against the temperature of the gases in the cylinder for 1,600 rpm; 50% throttle operation mode (medium power) when the engine was run on HVO. In Figure 8, the values of γ estimated from Eq. (1) to Eq. (4) that expressed γ (T) were graphically compared to the values that were evaluated using the modified gamma function, γ_{mod}. Gamma 1 to 4 were the gamma values predicted by Eq. (1) to Eq. (4) respectively. Figure 8 showed that the estimated values of γ from γ_{mod} at all temperature points were much higher than the estimates from the other functions which expressed γ as a function of temperature only. The same trend was observed for standard diesel and GTL diesel. Therefore, it can be concluded that λ has a significant effect on γ when alternative fuels are used in CI engines. Olanrewaju, F.O., et al., [2] also showed that λ had a significant effect on γ when the engine was run on off–road diesel.

The excess air ratio, λ was a constant value at each of the tested modes. The observed unusual rise in the values of γ predicted by γ_{mod} as the temperature increased above 1,000 K was due to the sensitivity of the polynomial γ model (Eq. (6)) to λ. The predicted γ values were observed to drop in the previous work by the authors as the temperature increased (the values of λ were > 2 in the previous work) [2]. In the current work, for values of λ < 2, γ dropped as the temperature increased to 1,000 K for all the fuels. At temperatures above 1,000 K, γ increased with increase in temperature for all the fuels when λ was < 2 (Figure 8). The same trends were observed for the alternative fuels

for values of λ < 2 and λ >2. However, the values of γ for pure diesel were observed to drop as temperature increased for values of λ > 2 in the previous work. The observed trend of γ for the alternative fuels differed from that of ULSD when λ was > 2.

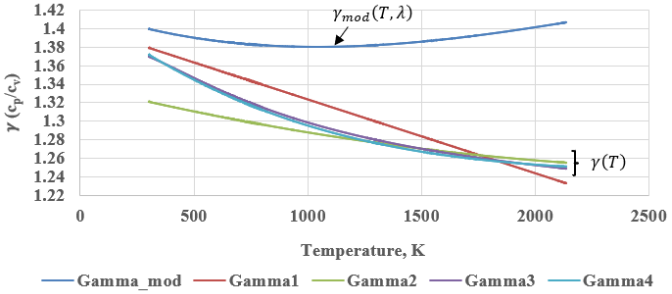

Figure 8. Comparison of modified gamma and gamma functions from literature (HVO: 1,600 rpm; 50% throttle_27 kW)

Sensitivity of diesel engine HRR model to γ functions - comparison of Leeds model to others

The HRR profiles from the investigated HRR models were presented as shown in Figures 9 to 17. The profiles for standard diesel were as depicted in Figures 9 to 11, while the HRR profiles for GTL and HVO diesels were as depicted in Figures 12 to 14, and Figures 15 to 17 respectively. The sensitivity of the HRR model of the engine to γ functions was vividly depicted by the figures as the five HRR models predicted different PHRR values. The Leeds HRR model predicted the lowest PHRR for all the modes that were tested for the three fuels. Figure 8 showed that $\gamma(T,\lambda)$ gave estimates of γ that were higher than the estimates from the functions that expressed $\gamma(T)$. However, figures 9 to 17 showed that, for both standard diesel and the alternative fuels, the HRR model that utilized $\gamma(T,\lambda)$ predicted lower PHRR values for the CI engine than the HRR models that utilized $\gamma(T)$. Though the five HRR models showed the same trend, they predicted different PHRR for each of the engine modes that was investigated. This necessitated the validation of the Leeds HRR model by comparing the fuel consumption of the engine predicted by the models to the measured fuel consumption in the next section.

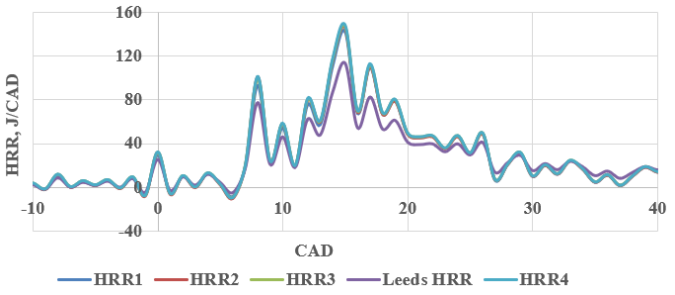

Figure 9. HRR profiles from the Leeds model and other models: standard diesel (1,000 rpm; 30% throttle_13 kW)

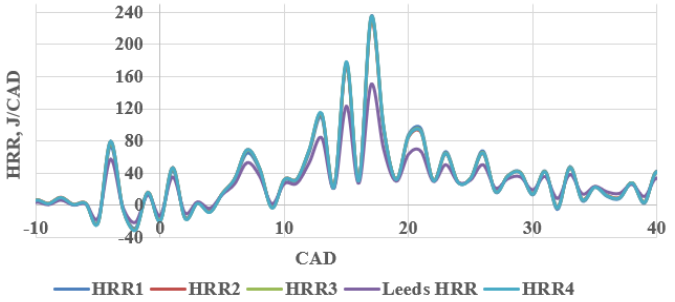

Figure 10. HRR profiles from the Leeds model and other models: standard diesel (1,600 rpm; 50% throttle_27 kW)

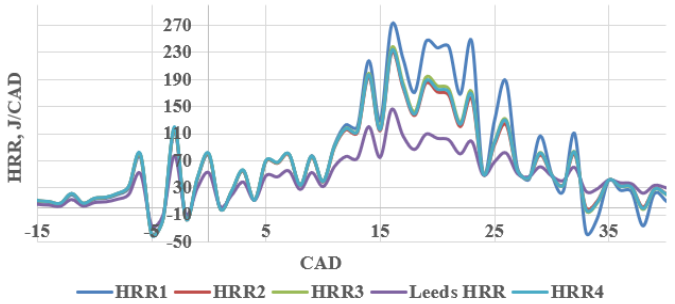

Figure 11. HRR profiles from the Leeds model and other models: standard diesel (1,900 rpm; 70% throttle_47 kW)

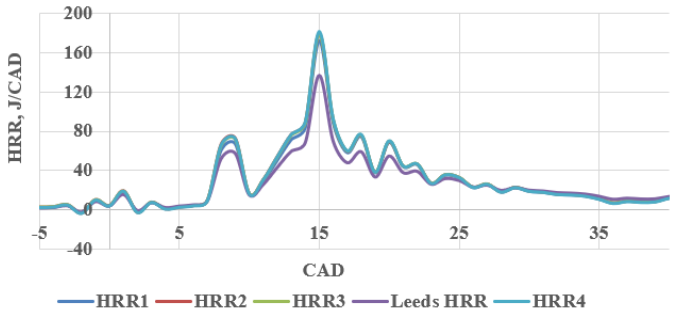

Figure 12. HRR profiles from the Leeds model and other models: GTL diesel (1,000 rpm; 30% throttle_13 kW)

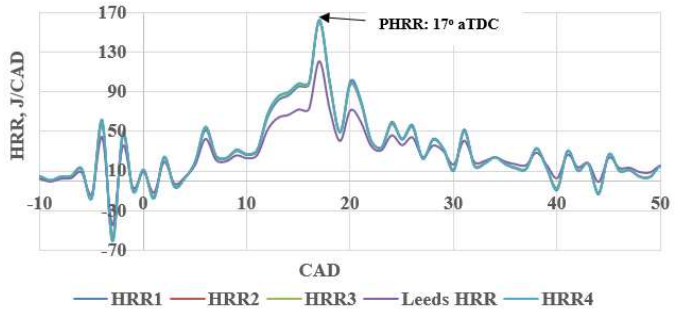

Figure 13. HRR profiles from the Leeds model and other models: GTL diesel (1,600 rpm; 50% throttle_27 kW)

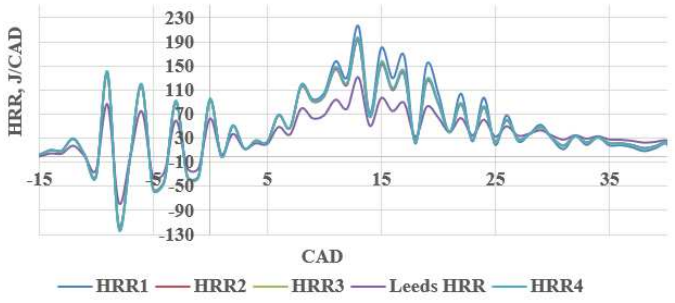

Figure 14. HRR profiles from the Leeds model and other models: GTL diesel (1,900 rpm; 70% throttle_47 kW)

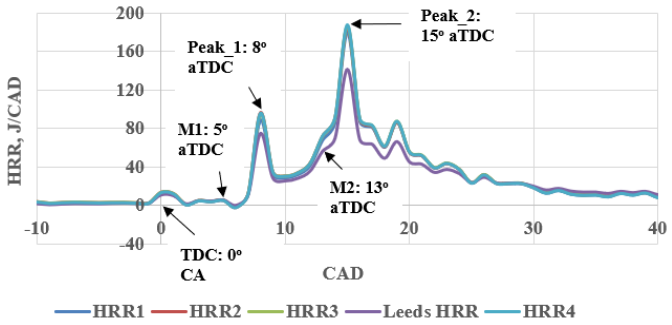

Figure 15. HRR profiles from the Leeds model and other models: HVO diesel (1,000 rpm; 30% throttle_13 kW)

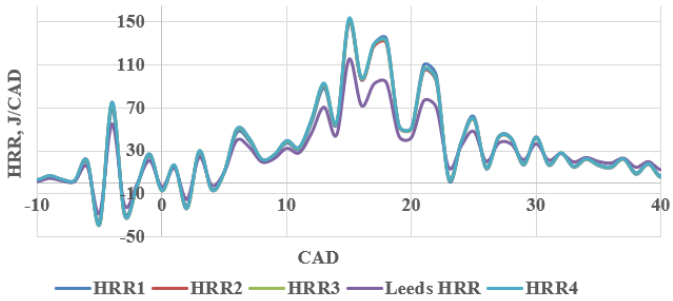

Figure 16. HRR profiles from the Leeds model and other models: HVO diesel (1,600 rpm; 50% throttle_27 kW)

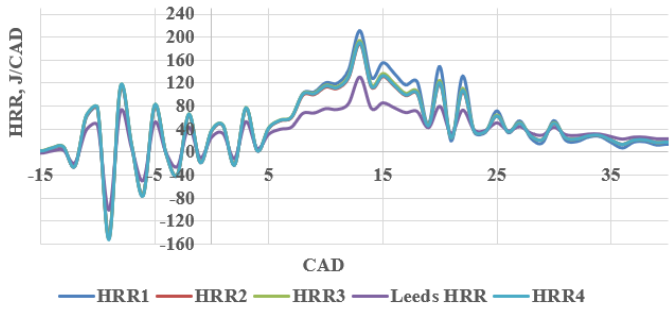

Figure 17. HRR profiles from the Leeds model and other models: HVO diesel (1,900 rpm; 70% throttle_47 kW)

The crank angle timing of the PHRR of the engine for each of the tested modes was determined directly from the HRR profile. As depicted in Figure 13, the PHRR for the 1,600 rpm; 50% throttle mode occurred at 17° aTDC for GTL diesel. Multiple peaks were also observed in all the HRR profiles as a result of the multiple fuel injection strategy of the engine. The 1,000 rpm; 30% throttle engine mode showed two prominent peaks for HVO diesel. Peak_1 resulted from the heat that was released from the combustion of the fuel that was injected during the pilot fuel injection and the first main injection, M1 (at 5° aTDC). Thereafter, there was another main injection event, M2 at 13° aTDC which caused another heat release that lead to the second prominent peak (Peak_2).

Validation of the Leeds HRR model

The Cumulative Heat Release (CHR) profiles shown in Figures 18 to 20 (strictly for the heat that was released as a result of the combustion of injected fuel) were determined from the HRR profiles. The HRR and CHR profiles of the fuels were used to predict the fuel consumption of the engine per thermodynamic cycle per cylinder. The figures present the heat that was released in each of the four cylinders per power stroke (in joules) from the combustion of the injected fuel mass.

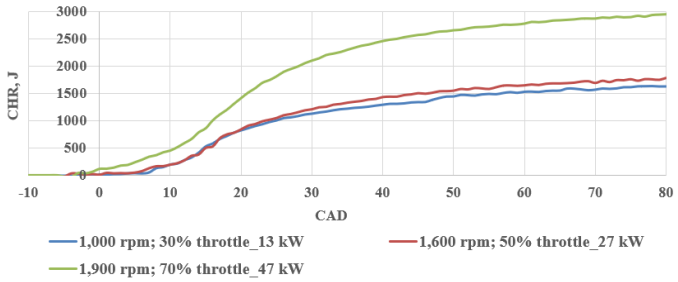

Figure 18. Cumulative heat release profiles (standard diesel)

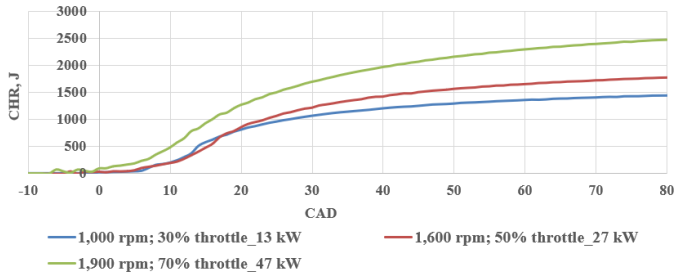

Figure 19. Cumulative heat release profiles (GTL diesel)

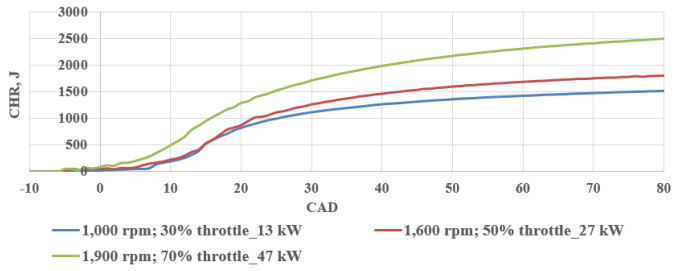

Figure 20. Cumulative heat release profiles (HVO diesel)

The result of the validation of the HRR models was presented graphically as shown in Figure 21. Figure 21 showed that the fuel masses predicted by the Leeds model (the pink bars with black borderline) were generally more accurate than the predictions from the other models for the investigated fuels and engine modes. The Leeds HRR model predicted the fuel consumption of the engine for ULSD, GTL and HVO diesels with an overall average (absolute) error of 4.86% compared to the measured fuel consumption (blue bars with black borderline). The percentage errors of the fuel masses predicted by the Leeds HRR model ranged from -8.27 to +8.69, with a standard deviation of 2.39. The overall average error that was obtained for off–road diesel using the Leeds HRR model was 1.41% [2]. The percentage error obtained in the current work was relatively high compared to the previous work because in the current work, multiple fuels with quite different HRR behaviours were investigated whereas the previous work predicted the fuel masses of a single fuel (off-road diesel). The overall average errors in the predicted fuel masses by the other HRR models that were based on $\gamma(T)$ ranged from 14.66% to 19.99%. The HRR models that were based on $\gamma(T)$ overpredicted the fuel consumption of the engine because the significant effect of λ on γ was not accounted for in the models. Figure 21 clearly showed that the accuracy of the HRR model of CI engines for predicting the combustion behaviour of standard diesel and the alternative fuels was enhanced by using $\gamma(T, \lambda)$. The incorporation of the rate of evaporation of the injected fuel into the Leeds HRR model (Eq. (8)) also contributed to the accuracy of the model.

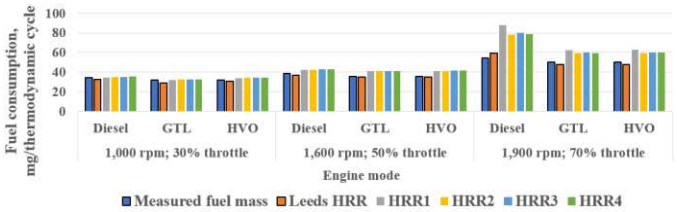

Figure 21. Comparison of measured and predicted fuel masses

The analysis that was done to compare the predicted fuel masses to the measured fuel mass was summarized as presented in Table A.2.

Determination of combustion phasing

The validated model (Leeds HRR model) was used to determine the SoC, EoC and the crank angle timing at which 50% of the injected fuel mass was burned (MFB50) from the fuel burn profiles for the fuels and the engine modes that were tested. The determination of the phasing of the combustion (SoC, MFB50, EoC) for a low power condition (1,000 rpm; 30% throttle for HVO diesel) and a high power condition (1,900 rpm; 70% throttle for ULSD) were presented as shown in Figure 22 and Figure 23. Figure 22 showed that, when the engine was run on HVO at low power (1,000 rpm; 30% throttle), the SoC was at 1° bTDC, 50% of the injected fuel was burned at 17° aTDC while the EoC was at 49° aTDC. At low and medium power conditions, the SoC could easily be determined from the HRR profile as there were no significant heat release and fluctuations from the combustion of pilot injection fuel. However, due to the significant heat release from the combustion of pilot injection fuel mass (pilot combustion) at the high power condition as observed in Figures 11, 14, and 17, two SoC crank angles: SoC1, and SoC2 were identified in the fuel burn profile for the high power conditions depicted in Figures 23 and 24. The quantity of fuel that was injected during the pilot fuel injection to achieve optimum charge premix and to minimize peak pressure and peak temperature was relatively high at the high power condition. This led to significant pilot combustion heat release before the TDC as observed in Figures 11, 14, and 17.

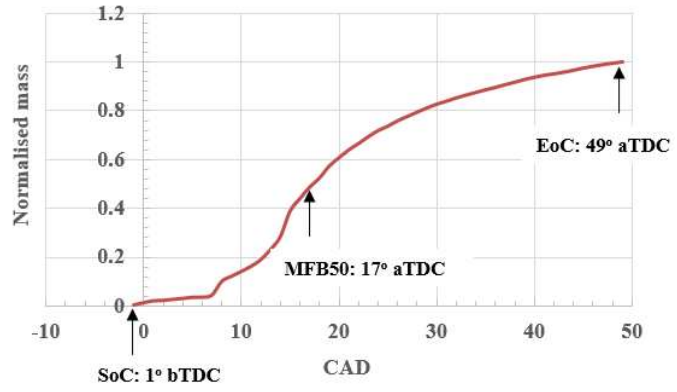

Figure 22. Determination of combustion phasing for HVO (1,000 rpm; 30% throttle_13 kW)

SoC1 was the start of pilot combustion while SoC2 was the actual (effective) start of combustion for the high power condition. The significant release of heat bTDC (seen as the fluctuation in the HRR profiles for the high power condition) was triggered by the advanced SoI for the high power condition. The fluctuations that were observed near the TDC in the pressure traces and temperature profiles (Figures 2 to 7) were amplified in the HRR profiles as the power of the engine increased. The crank angle at which the fluctuations began marked the start of fuel injection, SoI. SoC2 was determined so that the significant heat that was released bTDC for the high power condition could be accounted for thereby further increasing the accuracy of the Leeds HRR model. SoC2 could not be determined by direct inspection of the HRR curve alone. As such, it was determined from the fuel burn profile as shown in Figures 23 and 24. The fuel burn profiles that were generated from the HRR profiles resolved the fluctuations that were observed bTDC for the high power condition such that SoC2 was clearly distinguished from SoC1. As shown in Figures 23 and 24, SoC2 was the crank angle timing at which the MFB rose consistently above zero.

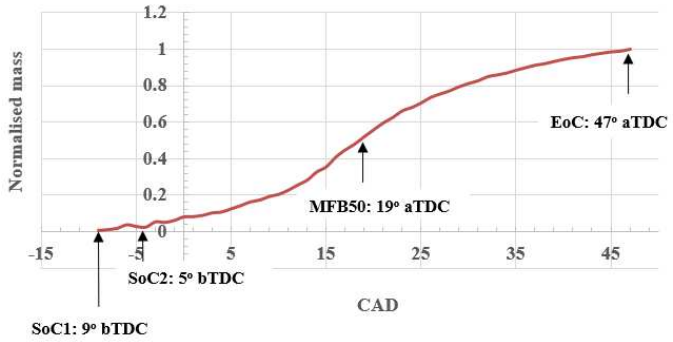

Figure 23. Determination of combustion phasing for ULSD (1,900 rpm; 70% throttle_47 kW)

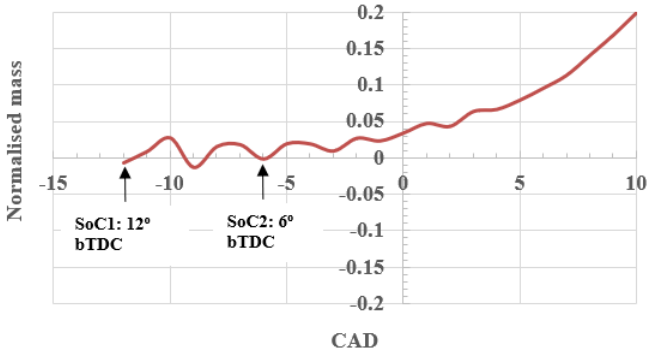

Figure 24. Determination of SoC1 and SoC2 for HVO (1,900 rpm; 70% throttle_47 kW)

SoC2 was clearly identified in Figures 23 and 24 as the point where the fuel burn profiles for ULSD and HVO diesel rose consistently above zero. As shown in Figure 23, SoC1 was 9° bTDC while SoC2 was 5° bTDC for ULSD. It could be seen from the fuel burn profile in Figure 24 that the MFB rose consistently above zero at 6° bTDC (SoC2) even though the combustion of the pilot injection HVO fuel commenced at 12° bTDC (SoC1). The MFB cannot be negative. Therefore, for the high load condition, SoC2 was chosen as the actual/effective SoC while SoC1 was designated as the start of pilot fuel combustion. The start of pilot combustion (SoC1) and the actual start of combustion (SoC2) for GTL diesel at the high power condition were 13° bTDC, and 7° bTDC respectively. The combustion phasing for the low and medium power conditions were determined as shown in Figure 22, while the combustion phasing of the fuels for the high power condition were determined as shown in Figures 23 and 24.

The phasing of the combustion for the three fuels were tabulated as shown in Table 5. The injection timings for the three fuels were not the same for all the modes as shown in Table 5. The injection event was controlled by the ECU of the engine. The estimated injection timings in Table 5 were the crank angle timings for the start of pilot injection. The observed early combustion of GTL and HVO was not only due to their relatively high CN, it was also due to the advanced injection of the alternative fuels by the ECU. Generally, the SoI values at the higher power conditions showed that the injection event occurred much earlier for the alternative fuels than for ULSD. At the high power condition, much higher compression pressure and temperature were attained as shown in Figures 2 to 7. Therefore, advanced injection of fuel was triggered by the ECU of the engine at the higher power

conditions to prevent undesirable high PPRR and PHRR, both of which could occur should the SoI and SoC be too close to the TDC. The SoI of the alternative fuels was advanced by the ECU because they had a higher CN than ULSD. Generally, as the power of the engine was increased, the SoI was advanced for all the fuels. This was to enhance lean combustion and efficient premixing of fuel and air to prevent high PPRR, PHRR and the formation of local rich zones which would lead to high THC, CO, and NOx emissions. Apart from the cylinder pressure and temperature, the fuel consumption of the engine also increased as the power of the engine increased. As such, to keep the combustion mixture lean ($\lambda > 1$), the ECU advanced the injection timing of the fuels as the power was increased so that the multiple injection events occurred over a relatively wide crank angle range at the higher power conditions.

Table 5. Combustion phasing of the fuels (ULSD, GTL, and HVO diesel) at the tested engine modes

Test	Test mode	Fuel	CAD					
			PP	PHRR	SoI	SoC	EoC	MFB50
1	1,000 rpm; 30% throttle	ULSD	17	15	-2	-1	50	18
		GTL	16	15	-3	-2	49	17
		HVO	19	15	-2	-1	49	17
2	1,600 rpm; 50% throttle	ULSD	18	17	-6	-5	56	19
		GTL	18	17	-8	-5	48	19
		HVO	18	15	-8	-5	47	18
3	1,900 rpm; 70% throttle	ULSD	20	16	-10	-5	47	19
		GTL	13	13	-14	-7	46	16
		HVO	13	13	-13	-6	46	16

Generally, for the three fuels that were investigated, Table 5 showed that as the power of the engine increased, the SoI and SoC of the fuels were advanced (occurred earlier). The auto-ignition of the diesel fuels was enhanced by the relatively high compression pressure and temperature which were attained in the cylinder as the power of the engine increased.

The Peak Pressures (PP) and the PHRR were determined from the pressure traces and the modelled HRR profiles respectively for the tested modes and fuels. The values of the PP and the PHRR for the tested modes were summarized as shown in Table 6.

Table 6. Model results for Peak Pressures (PP) and PHRR at the tested engine modes

Engine test mode	Fuel	PP, bar	PHRR, J/CAD
1,000 rpm; 30% throttle	ULSD	61.24	113.69
	GTL	58.23	136.70
	HVO	58.49	141.71
1,600 rpm; 50% throttle	ULSD	68.40	150.14
	GTL	66.48	121.15
	HVO	68.35	114.79
1,900 rpm; 70% throttle	ULSD	102.60	146.25
	GTL	102.64	131.01
	HVO	103.23	131.08

Smoothness of combustion of fossil diesel and alternative diesels

The smoothness of the combustion of standard diesel (ULSD) and the alternative fuels was also analyzed from the HRR profiles by superimposing the HRR profiles of the three fuels at the tested low, medium and high power conditions as shown in Figures 25 to 27. The figures showed that the combustion of HVO diesel in the engine was smoother than the combustion of standard diesel or GTL diesel. The HRR profiles of HVO diesel (the black curve) in the figures were not as wavy (noisy) as those of the other fuels. This could be attributed to the narrow distillation range of HVO (Figure 1). As depicted in Figures 25 to 27, as the power of the engine increased from low to high power, the tendency of the compressed charge to combust before the TDC increased. There was more combustion of pilot injection fuel (early SoC before TDC) when the engine was run on the alternative fuels than when it was run on ULSD. Consequently, to keep the actual SoC near the TDC as much as possible, the Engine Control Unit (ECU) suppressed the combustion of the pilot injection fuel by causing more fuel masses of GTL and HVO diesel to be injected before the TDC compared to the pilot injection fuel mass of ULSD. This multiple fuel injection strategy of the ECU was also aimed at preventing the PHRR from occurring before the TDC for the fuels with high CN. This would have a negative impact on the efficiency of the engine due to the early release of the chemical energy of the fuel before the actual commencement of the power stroke.

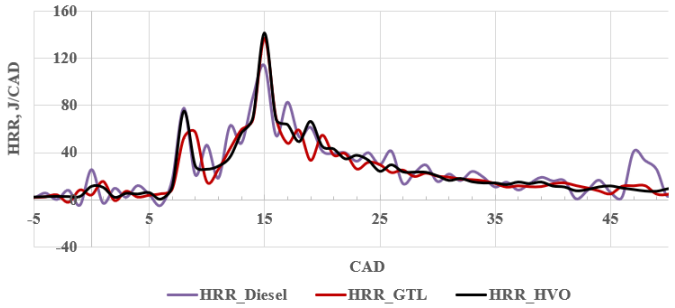

Figure 25. Comparison of the smoothness of combustion of ULSD, GTL, and HVO diesel (1,000 rpm; 30% throttle)

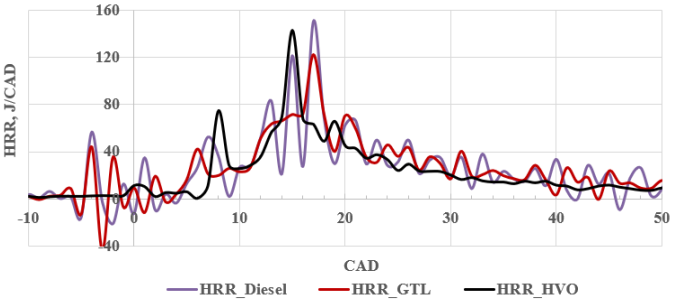

Figure 26. Comparison of the smoothness of combustion of ULSD, GTL, and HVO diesel (1,600 rpm; 50% throttle)

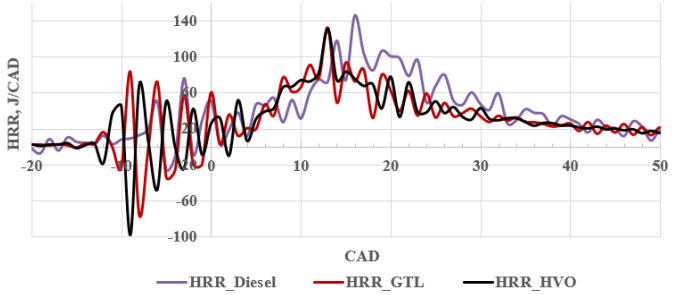

Figure 27. Comparison of the smoothness of combustion of ULSD, GTL, and HVO diesel (1,900 rpm; 70% throttle)

The PHRR was highest for ULSD at the higher power conditions (Figure 27 and Table 6) due to the relatively late SoI and low CN of ULSD that led to relatively late SoC as well as low pilot combustion heat release when the engine was run on ULSD. The start of pilot combustion (SoC1) for ULSD at the high power condition was 9° bTDC while the SoC1 were 13° bTDC and 12° bTDC respectively for GTL and HVO diesel fuels at the high power condition (Figures 11, 14, and 17). This implied that, at the high power condition for GTL diesel, pilot combustion started 4 CAD earlier than for diesel. Pilot combustion started 3 CAD earlier than it started for ULSD at the same condition (1,900 rpm; 30% throttle) when the engine was run on HVO diesel. The relatively low PHRR values of GTL and HVO diesel fuels compared to ULSD at the high power condition was due to the significant release of heat that occurred during the pilot combustion of the alternative fuels as explained in the previous section.

Summary/Conclusions

In this work, an improved HRR model – Leeds HRR model - was used to analyze the HRR of standard diesel, GTL and HVO diesels in a multiple fuel injection strategy, CI (diesel) engine. No work has been done in the past to model and analyze the HRR of the alternative diesel fuels in a multiple fuel injection strategy, CI (diesel) engine. The current work has shown that the accuracy of the HRR models of CI engines for both fossil and alternative diesel fuels is strongly depended on the specific heats ratio (γ). The effect of the excess air ratio (λ) on γ was investigated in this work. λ was found to have a significant effect on γ for the three fuels that were investigated. Therefore, in the current work, a modified γ function, $\gamma_{mod}(T,\lambda)$ was used in the Leeds HRR model to model the HRR of the three fuels. The Leeds HRR model predicted the fuel consumption of the engine for ULSD, GTL and HVO diesels with an overall average (absolute) error of 4.86% compared to the measured fuel consumption. The errors in the fuel masses predicted by the Leeds HRR model ranged from -8.27% to +8.69%, with a standard deviation of 2.39. The average error in the fuel mass predictions of the other models which were based on $\gamma(T)$ ranged from 14.66% to 19.99%. The errors in the predictions of the other models were high because λ was neglected in the models. Therefore, in this work, it was shown that the accuracy of the HRR model of CI engines for the determination of the combustion behaviour of fossil and alternative diesel fuels is enhanced by using $\gamma(T,\lambda)$. The PHRR was highest for ULSD at the high power condition due to the relatively late SoI and low CN of ULSD compared to GTL and HVO diesels. The combustion of HVO diesel was found to be the smoothest of the three fuels due to the narrow distillation range of HVO diesel. The novel techniques that were used to estimate the rate of evaporation of the injected fuels from the HRR profiles and the actual SoC from the HRR and fuel burn profiles (for the case of significant heat release bTDC) also contributed to the accuracy of the Leeds HRR model.

References

1. Ceviz, M. A., and Kaymaz, I., "Temperature and air–fuel ratio dependent specific heat ratio functions for lean burned and unburned mixture," *Energy Conversion and Management* 46(15):2387-2404, 2005, doi: 10.1016/j.enconman.2004.12.009.
2. Olanrewaju, F. O., Hu, L., Gordon, E. A., and Herodotos N. P., "Improved model for the analysis of the Heat Release Rate (HRR) in Compression Ignition (CI) engines," *Journal of the Energy Institute*, 2020, doi: 10.1016/j.joei.2020.04.005.
3. Wu, Y., Jason F., Hu L., and Gordon A., "Investigation of Combustion and Emission Performance of Hydrogenated Vegetable Oil (HVO) Diesel," *SAE Int. J. Fuels Lubr.* 10(3): 2017, doi: 10.4271/2017-01-2400.
4. Abu-Jrai, A., Tsolakis, A., Theinnoi, K., Cracknell, R., et al., "Effect of Gas-to-Liquid Diesel Fuels on Combustion Characteristics, Engine Emissions, and Exhaust Gas Fuel Reforming. Comparative Study," *Energy & Fuels* 20 (6):2377-2384, 2006, doi: 10.1021/ef060332a.
5. Gatowski, J. A., Balles, E. N., Chun, K. M., Nelson, F. E., et al., "Heat Release Analysis of Engine Pressure Data," *SAE Int. J. Fall Fuels Lubr.*, 1984, doi: 10.4271/841359.
6. Brunt, M. F. J., and Andrew L. E., "Evaluation of Burn Rate Routines and Analysis Errors," *SAE Int. J.*, 1997, doi: 10.4271/970037.
7. Egnell, R., "Combustion Diagnostics by Means of Multizone Heat Release Analysis and NO Calculation," *SAE Int. J. Fuels Lubr.*, 1998, doi: 10.4271/981424.
8. Blair, G.P., "The Basic Design of Two-stroke Engines," (Warrendale, SAE International, 1990), ISBN: 1-56091-008-9.
9. Heywood, J. B., "Internal combustion engine fundamentals," (New York, McGraw-Hill, Inc., 1988), ISBN: 978-0-07-028637-5.
10. AVL, "GCA Gas Exchange and Combustion Analysis," (Germany, AVL, 2015).
11. Smith, M., "Unit Injectors and Common Rail Fuel Injection Systems," presented at Delphi Diesel Systems 2012, UK, May 18, 2012.
12. Hohenberg, G. F., "Advanced Approaches for Heat Transfer Calculations," *SAE Int. J. Off-Highway and Powerplant*, 1979, doi: 10.4271/790825.
13. NCH Europe, "EN590 diesel fuel requirements in the EU," https://www.ncheurope.com/en/diesel-requirements-eu, accessed Apr. 2020.
14. Sajjad, H., Masjuki, H.H., Varman, M., Khan, M. M. R., et al., "Comparative Study of Biodiesel GTL Fuel and their blends in Context of Engine Performance and Exhaust Emission," *Procedia Engineering* 90(2014): 466-471, 2014, doi:10.1016/j.proeng.2014.11.758
15. Reyes, J. G. T., and Quiros, E. N., "Determination of the Start and End of Combustion in Direct Injection Diesel Engine Using the Apparent Heat Release Rate," presented at POWER-ICOPE2017-3446, USA, June 26-30, 2017.

Contact Information

Francis Omotola Olanrewaju
School of Chemical and Process Engineering, (SCAPE)
University of Leeds.
Email: pmofo@leeds.ac.uk
Tel.: +447503114068; +2347030285759

Acknowledgments

This work was funded by the Petroleum Technology Development Fund (PTDF), Nigeria and supported by the National Agency for Science and Engineering Infrastructure (NASENI), Nigeria. We would like to thank the Shell International Petroleum Company Limited for supplying the GTL fuel. We also appreciate Mr. Scott Prichard for his technical support and expertise.

Definitions/Abbreviations

A_{eff}	Effective flow area
A_s	Surface area
a_i	Coefficients of ratio of specific heats function for unburned mixtures.

b_1	Coefficients of ratio of specific heats function for burned mixtures.
c_m	Mean piston speed
c_v	Specific heat capacity at constant volume
HCCI	Homogeneous Charge Compression Ignition
h	Heat transfer coefficient
h_{bb}	Enthalpy of blow-by gases
K_1	Constant
m	Amount of gas in cylinder
m_{bb}	Mass of blow-by gases
m_f	Mass of injected fuel
p	Pressure
Q	Heat release from injected fuel
Q_b	Heat loss through blow-by gases
Q_w	Heat loss through cylinder walls
q_e	Heat of evaporation of fuel
R	Universal gas constant
T	Temperature
t	Time
U	Internal energy
V	Volume
W	Pressure-volume (pV) work
wt	Weight
γ	Ratio of specific heats
δ	Blow-by gap
k_1, k_2	Constants
λ	Excess air ratio
ϕ	Equivalence ratio
ρ	Density
θ	Crank Angle Degree
$\omega_1, \omega_2, \omega_3$	Constants
b	Burned mixture
bb	Blow-by
e	Evaporation
mod	Modified
ref	Reference
s	Surface
u	Unburned mixture
w	Wall
aTDC	After Top Dead Centre
bTDC	Before Top Dead Centre
CAD	Crank Angle Degree
CHR	Cumulative Heat Release
CI	Compression Ignition
CN	Cetane Number
DI	Direct Injection
ECU	Engine Control Unit
EGR	Exhaust Gas Recirculation
EoC	End of Combustion
EVC	Exhaust Valve Closing
GTL	Gas-to-Liquid
HRR	Heat Release Rate
HVO	Hydrotreated Vegetable Oil
ICE	Internal Combustion Engine
IVC	Intake Valve Closing
MFB	Mass Fraction Burned
NCV	Net Calorific Value
PHRR	Peak Heat Release Rate
PP	Peak Pressure
PPRR	Peak Pressure Rise Rate
rpm	Revolutions per minute

SI	Spark Ignition
SoC	Start of Combustion
ULSD	Ultra Low Sulphur Diesel

Appendix

Table A.1. Coefficients for use in Equations 5, and 6

Coefficients (γ_u)	Values	Coefficients (γ_b)	Values
a_1	1.464202464	b_1	1.498119965
a_2	-0.000150666	b_2	-0.00011303
a_3	-7.34852e-08	b_3	-0.26688898
a_4	1.55726e-10	b_4	4.03642e-08
a_5	-7.6951e-14	b_5	0.273428364
a_6	1.19535e-17	b_6	5.7462e-05
a_7	-0.063115275	b_7	-7.2026e-12
		b_8	-0.08218813
		b_9	-1.3029e-05
		b_{10}	2.35732e-08

Table A.2. Summary of model validation results

			Fuel mass, mg/thermodynamic cycle						% Deviation from measured fuel mass				
Engine mode	Fuel	Lambda, λ	Measured	Leeds HRR	HRR1	HRR2	HRR3	HRR4	Leeds HRR	HRR1	HRR2	HRR3	HRR4
1,000 rpm; 30 % throttle (Low load)	USLD	1.80	34.57	32.82	34.71	35.27	35.27	35.42	-5.06	0.41	2.03	2.04	4.46
	GTL	1.87	31.78	29.15	31.95	32.62	32.57	32.72	-8.27	0.52	2.63	2.49	2.95
	HVO	1.91	31.78	30.59	33.80	34.47	34.44	34.59	-3.74	6.34	8.46	8.36	8.85
1,600 rpm; 50 % throttle (Medium load)	USLD	1.60	38.89	36.78	42.58	42.59	42.75	42.85	-5.43	9.48	9.50	9.93	10.19
	GTL	1.66	35.75	35.10	40.84	40.97	41.14	41.26	-1.81	14.24	14.60	15.06	15.43
	HVO	1.70	35.75	35.34	41.25	41.32	41.50	41.62	-1.14	15.38	15.57	16.07	16.41
1,900 rpm; 70 % throttle (High load)	USLD	1.14	54.58	59.32	88.02	78.05	79.71	79.01	8.69	61.27	43.01	46.05	44.76
	GTL	1.19	50.17	47.52	62.68	59.05	59.86	59.54	-5.28	24.93	17.70	19.31	18.68
	HVO	1.21	50.17	47.99	63.05	59.40	60.21	59.89	-4.35	25.68	18.40	20.01	19.38
					Average of absolute errors:				4.86	19.99	14.66	15.48	15.46
					Standard deviation:				2.39	17.71	11.53	12.48	11.94
					Error range:				-8.27 - +8.69	0.41 – 61.27	2.03 - 43.01	2.04 – 46.05	2.46 - 44.76